Supporting Information

Advanced Room-Temperature Cured Encapsulant Film for Crystalline Silicon Solar Modules: Enhancing Efficiency with Luminescent Down-Shifting, Flame Retardancy, and UV Resistance

Shuang Qiu, Huaibo Qian, Jun Sun, Xiaoyu Gu, Haiqiao Wang, Sheng Zhang**

State Key Laboratory of Organic-Inorganic Composites, Beijing University of Chemical Technology, Beijing 100029, China

E-mail: sunj@mail.buct.edu.cn; zhangsheng@mail.buct.edu.cn

Experimental Section

1.1 Materials

Silicone-acrylate emulsion (SA, QS-996, 48%, 1000-4000cps) was purchased from Polymer Applied Chemical New Material Co., Ltd. Sodium metasilicate pentahydrate (Na_2SiO_3, 95%), sodium fluorosilicate (Na_2SiF_6, 98%), ammonium polyphosphate (APP, n< 20, water solubility> 90g/100ml), m-Phenylenediamine (PD, 99%) were obtained from Macklin Co., Ltd. Other coating auxiliaries were provided by Trusted Chemical Industry Co., Ltd. All reagents were used without further purification.

1.2 Preparation process of APCDs:

APCDs were prepared via a hydrothermal method in aqueous solution using APP and PD (see **Figure S1**). Firstly, 0.184 g of PD and 0.194 g of APP were dissolved in 10 mL of deionized water and sonicated for 30 min. Secondly, the mixture was transferred to a 50 mL PTFE hydrothermal reactor and heated at 180°C for 10 h. When the reaction was completed, the solid precipitate was filtered out with 0.22 μm filter paper and the clarified solution was collected. Then, the supernatant was dialyzed in water for 48 h (with a 1000 Da molecular weight dialysis bag) and freeze-dried to obtain APCDs powder.

1.3 Preparation process of CAS/APCDs emulsion:

Firstly, a certain amount of SA emulsion, Na_2SiO_3, and deionized water was weighed in a beaker and heated to 50°C in a water bath. The additives (dispersant, defoamer, and thickener) were added slowly under stirring with suitable proportions and stirred continuously for 1.5 h until the solution was mixed uniformly. Then, a portion of Na_2SiF_6 and different ratios of APCDs were slowly mixed into the mixture and stirred for 30 min to obtain the final CAS/APCDs emulsion. The specific synthesis formula is shown in **Table S1.**

Table S1. Formulation for CAS/APCDs adhesive films

Sample	SA (wt%)	Na_2SiO_3 (wt%)	Na_2SiF_6 (wt%)	APCDs (wt%)	Auxiliaries (wt%)	Water (wt%)
CAS	50	10	1	0	2	rest[#]

CAS/0.5APCDs	50	10	1	0.25	2	rest
CAS/1.0APCDs	50	10	1	0.50	2	rest
CAS/1.5APCDs	50	10	1	0.75	2	rest

The remaining weight percentage is the water content.

1.4 Fabrication of CAS/APCDs adhesive film: The emulsion described above was concentrated and thickened by heating it in an oven at 70°C. The concentrated emulsion was then uniformly applied to a PTFE plate using a laboratory applicator and dried naturally to obtain the CAS adhesive film sample. Similarly, the concentrated emulsion was uniformly scraped on one side of the glass plate, and a commercial single crystalline silicon solar cell was covered on the glass plate. The module was ventilated at room temperature until the adhesive film was formed. Subsequently, the whole module was placed in an oven at 70°C overnight to ensure that the moisture in the film evaporated sufficiently.

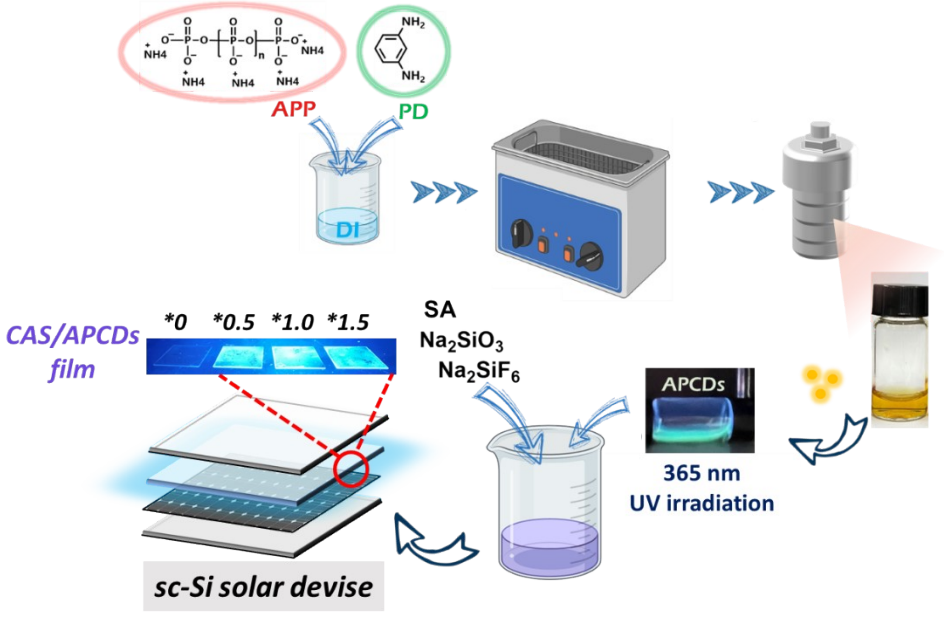

Figure S1. Schematic illustration for the preparation of APCDs and CAS composite adhesive films (* indicates the mass percentage of APCDs in the SA emulsion).

1.5 Characterization: Fourier transform infrared (FTIR) spectra were obtained by a Nicolet Nexus 670 FTIR spectrometer using a resolution of 4 cm^{-1} and 32 scans with a KBr disc. The attenuated total refraction (ATR) infrared reflectance spectra of adhesive

films were obtained in a Nicolet IS5 by scanning 128 times within the range of 4000-550 cm^{-1}. The physical phases of the samples were analyzed using an X-ray diffractometer (XRD, D8 Advance) with Cu Kα as the radiation source. X-ray photoelectron spectra (XPS) were obtained using an ESCALAB 250 spectrometer (ThermoVG) under a monochromatic Al Kalph 150 light source. The morphology of APCDs and CAS films was investigated using a JEM-2100F transmission electron microscope (TEM) and a Hitachi S-4700 scanning electron microscope (SEM). The tensile properties of CAS films were evaluated on a CMT4104 pulling machine (SANS Company), with a tensile speed of 10 mm/min. According to ISO 1184-1983, 5 samples were measured at ambient temperature to obtain the average value. The adhesive strength of CAS adhesive film was evaluated by the Instron 3366 universal testing machine (*Instron* Corp.). The CAS adhesive film was applied to a 4 mm × 25 mm × 65 mm glass plate with a bond area of 25 mm × 25 mm. The test was conducted at a tensile speed of 10 mm/min, according to the standard GB/T 17657-2013. The Limiting Oxygen Index (LOI) test was conducted according to ASTM D2863-17 using a Jiangning JF-3 instrument, with the sample tailored to 130 mm × 6.5 mm × 1.6 mm. The UL-94 vertical combustion test was performed using a Jiangning CZF-3 instrument according to ASTM D3801-2010, with a sample size of 130 mm × 13 mm × 1.6 mm. The combustion behavior of CAS films was characterized using a cone calorimeter (CC, Phoenix Instruments). The tests were carried out on specimens with dimensions of 100 mm × 100 mm × 1.6 mm at a heat flux of 35 kW according to ISO 5660. Fire performance index (FPI) and fire growth index (FGI) were calculated as follows:

$$FPI = \frac{time\ to\ ignition\ (TTI)}{peak\ of\ heat\ release\ (pHRR)} \quad (1)$$

$$FGI = \frac{pHRR}{time\ to\ pHRR} \quad (2)$$

UV-Vis absorption spectra of the samples were measured by a UV-Vis absorption spectrometer (UV-3600, SHIMADZU). The attached glass plates with CAS films were placed in the UV-visible spectrometer equipped with an InGaAs detector and integrating sphere for transmittance testing. Photoluminescence spectra and

fluorescence decay curve of APCDs were obtained with an Edinburgh FLS1000 spectrofluorometer. The refractive index (n) of the samples was examined using an ellipsometer (IR-VASE Mark II M-2000UI). For natural light incident on a substrate, the reflection at the interface of the two media could be obtained from Fresnel's formula as follows:[1]

$$R = \left(\frac{n_s - n_0}{n_s + n_0}\right)^2 \quad (3)$$

Where R was the reflectivity, n_s and n_0 were the refractive index of the upper and lower substrate, respectively. On the assumption that light was incident perpendicularly and that the modes of the vectors R_1 and R_2 were equal, the optimum n of the antireflective film (n_1) could be obtained from Eq. (4)-(5):[2]

$$R_1 = R_2, \left|\frac{n_1 - n_0}{n_1 + n_0}\right| = \left|\frac{n_s - n_1}{n_s + n_1}\right| \quad (4)$$

$$n_1 = (n_o \times n_s)^{\frac{1}{2}} \quad (5)$$

As for the influence of CAS adhesive film on the photovoltaic performance of Si solar cells, experimental samples were prepared by scraping CAS adhesive films onto one side of a 2.5 cm × 2.5 cm coverslip and then gluing to the upper surface of a commercial sc-Si solar cell (2.2 cm × 2.2 cm). The J-V curves of the sc-Si solar cells were characterized with a solar module analyzer (PROVA-210) under a PLS-SXE300D xenon light source. In order to investigate the photon response of solar cells at various wavelengths and to validate the reliability of the photocurrent obtained from J-V measurements, external quantum efficiency (EQE) measurements were further conducted using a CEL-QPCE3000 photoelectrochemical quantum efficiency test system. The surface average temperature of the CAS films were measured by an infrared thermal imager (TIS20+, FLUKE). To investigate the UV resistance of CAS films, specimens with a thickness of 250 μm were placed in a UV aging chamber at a constant temperature of 60°C equipped with a 300 W 320 nm UV light source. The surface topography of aged samples was recorded by an optical microscope (BX53, Olympus).

According to the Van 't Hoff Equation, the chemical reaction rate varied with temperature; i.e., for every 10°C increased in temperature, the reaction rate usually increased by a factor of between 2 and 3.[3] Assuming a factor value of 2.5, an extrapolation of the laboratory-simulated UV irradiation converted to actual daylight radiation time was performed. The reaction acceleration multiplicity estimated following the factor and the total energy output of the laboratory-simulated UV lamp after acceleration were calculated below:

$$\mu_{ad} = 2.5^{\frac{(T_R - T_0)}{10}} \quad (6)$$

$$E_{UV-ad} = E_{UV} \times t_i \times \frac{3600s}{h} \times \mu_{ad} \quad (7)$$

Where μ_{ad} denoted the adjusted multiplicative increase in the reaction rate, and T_R and T_0 were the laboratory simulation temperature and an ambient room temperature of 25°C; E_{UV} represented the UV lamp power, E_{UV-ad} represented the total energy of the adjusted laboratory-simulated UV irradiation, and t_i was the laboratory-simulated light time. Based on the assumption that the total radiant power of actual sunlight (I_S) was 1000 W/m², of which UV-A was about 3%, the formula for converting the laboratory simulated aging time into daylight exposure time per 1m² area (t_s) was as follows:

$$t_s = \frac{E_{UV-ad}}{I_S * 0.03 * 1 * 3600s/h} \quad (8)$$

1.6 Finite difference time domain (FDTD) simulation: The reflectance and light field distributions of different microstructures on crystalline Si solar cells were numerically analyzed by Ansys Lumerical FDTD simulations.[4] In the modeling, the refractive index data of CAS films and APCDs tested with ellipsometry were imported in advance. The n of the glass and silicon nitride (SiNx) coating were taken from the built-in data of the FDTD system. The modeling was carried out according to the structure shown in **Figure S2**. A planar light source with wavelengths ranging from 400 nm to 1100 nm was chosen to simulate visible light propagating downwards along the z-axis. The

dimension of the simulation unit was 2.7 μm × 2.7 μm × 2.2 μm, and the mesh size was 3 nm × 3 nm × 10 nm. Perfectly matched layer (PML) boundary conditions were imposed on the x-axis, y-axis (in-plane), and z-axis (out-of-plane) of the FDTD. The reflection results were obtained by time-domain integration of the pointing vectors at the input ports.

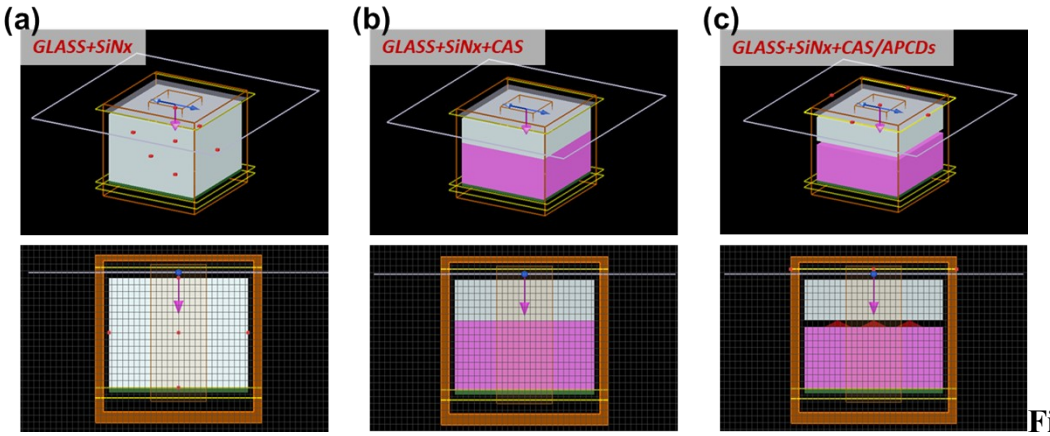

Figure S2. Schematic illustrations of the models based on FDTD simulation.

Results and Discussion

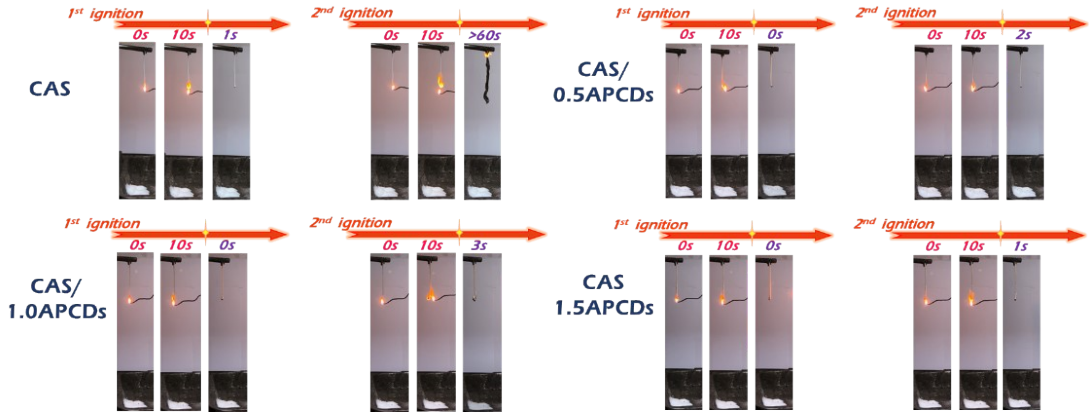

Figure S3. Screenshot of UL-94 vertical combustion test of CAS/APCDs adhesive film.

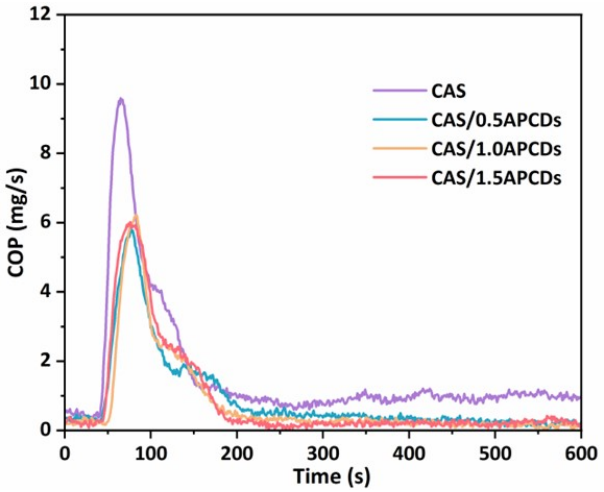

Figure S4. CO release curve of CAS composite films.

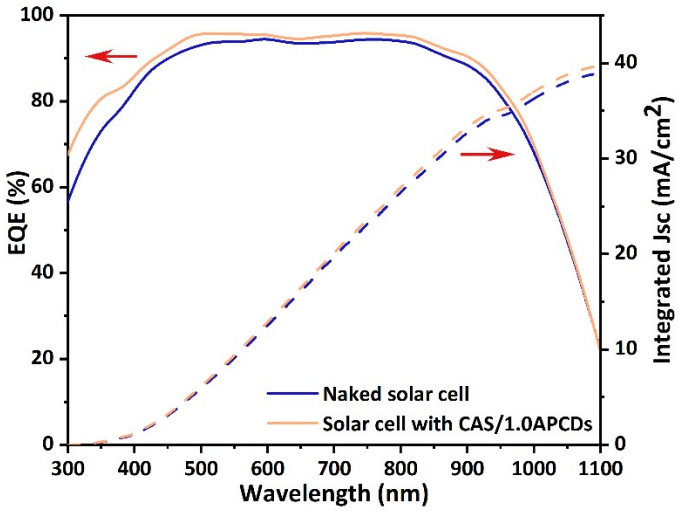

Figure S5. EQE characterization and integrated Jsc from EQE of solar cell before and after coated with CAS/APCDs film.

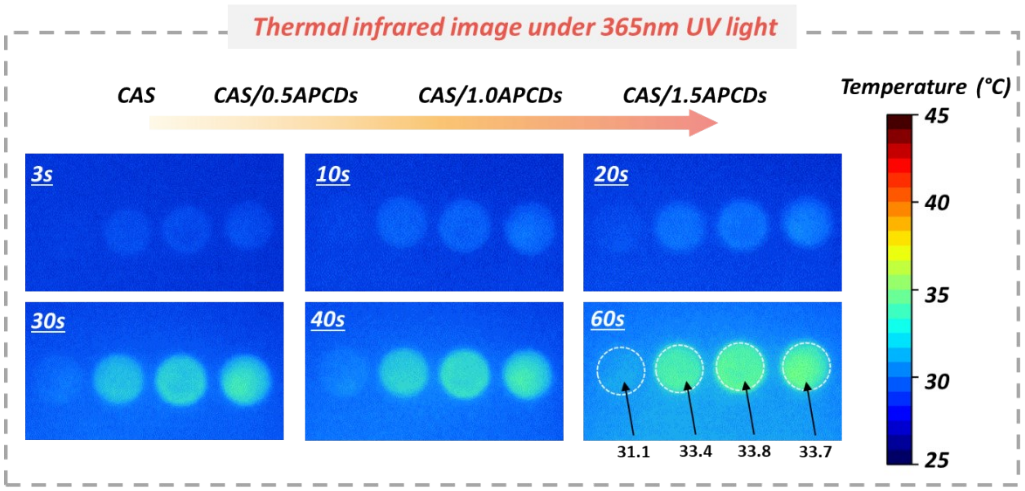

Figure S6. Thermal infrared imaging photographs of CAS films under UV irradiation.

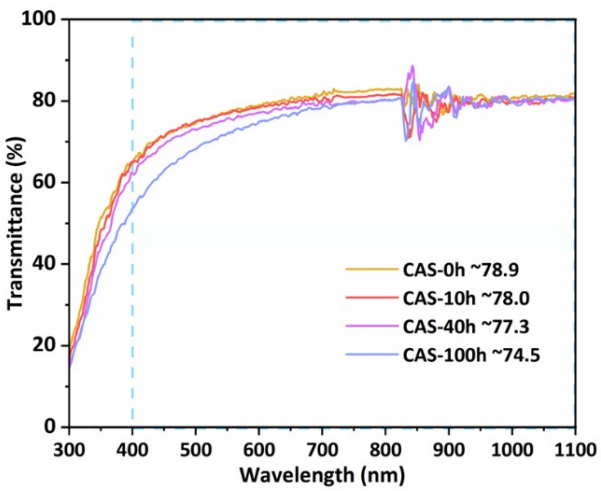

Figure S7. Transmittance of CAS films under different UV irradiation times.

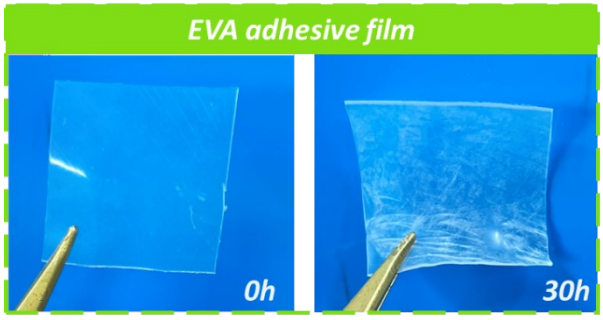

Figure S8. Surface photographs of EVA adhesive film before and after UV aging.

Table S2. LOI and UL-94 test data for CAS and CAS/APCDs adhesive film.

Sample	LOI (%)	Vertical combustion test (UL-94)		
		Classifications	Melt dripping	t_1/t_2 (s)
CAS	29.3±0.1	NR*	No/No	1/>60
CAS/0.5APCDs	32.0±0.1	V-0	No/No	0/2
CAS/1.0APCDs	32.6±0.2	V-0	No/No	0/3
CAS/1.5APCDs	33.5±0.2	V-0	No/No	0/1

*NR means no rating.

Table S3. Influence of the CAS/APCDs adhesive film (thickness = 10 μm) on the PV performance of the sc-Si solar cells.

	Jsc (mA/cm^2)	Voc (V)	Power (mW/cm^2)	PCE (%)	ΔJsc (%)	ΔPCE (%)	Fill Factor
Naked Si-solar	38.15 ± 0.18	0.587±0.007	14.71	14.71	-	-	0.656
Si-solar coated with CAS film	37.03 ± 0.20	0.561± 0.006	13.76	13.76	-2.9	-6.4	0.654
Si-solar coated with CAS/0.5APCDs film	41.03± 0.11	0.558± 0.008	14.99	14.99	7.5	1.9	0.657
Si-solar coated with CAS/1.0APCDs film	39.47± 0.17	0.566± 0.006	15.55	15.55	3.5	5.7	0.679
Si-solar coated with CAS/1.5APCDs film	39.23± 0.15	0.560± 0.003	14.65	14.65	2.8	-0.4	0.669

Table S4. Comparison of the present work with recent studies on LDS layers prepared from carbon dots.

	J_{SC} (mA/cm^2)	V_{OC} (mV)	PCE (%)	Fill Factor (%)	ΔJ_{SC} (%)	ΔFF (%)	ΔPCE (%)	DOI	Year
Solar module without film	40.03 (ΔI_{SC},mA)	2328	16.69	71.65	1.3 (ΔI_{SC}, %)	-0.3	1.2	10.1021/acsanm.0c00175	2020
0.2%QD@EVA Films	40.57	2331	16.89	71.43					
Si solar cell without layer	31.83	616	14.15	72.18	3.0	0.02	7.1	10.1039/d1se00142f	2021
BCNO silica gel-based LDS layer	32.80	617	14.60	72.20					
c-Si SC	35.82 ± 0.018	610 ± 12	17.39 ± 0.051	79.5	5.8	-0.1	5.8	10.1021/acsami.9b21087	2020
With 0.03%NR-CQDs	37.92 ± 0.017	610 ± 11	18.41 ± 0.050	79.4					
Solar Cell Set	36.58	613	15.27 ± 0.21	68.10	0.6	1.5	2.2	10.1016/j.mee.2019.111047	2019
PMMA+10 μM Chl-A film	36.80	612	15.61 ± 0.21	69.14					
Control module	35.47	620	17.44	79.36	1.4	0.4	2.4	10.1002/pip.3109	2019
Module with CQD-SI	35.98	620	17.86	79.69					

c-Si SC	31.5	592	13.1	70	1.4	0	2.3	10.1016/j.matlet.2020.128515	2020
With 1 GQDs Layers	31.94	601	13.4	70					
Bare cell	6.689	2381	11.998	75.327	0.3	0.06	2.0	10.1021/acs.jpclett.2c03632	2023
Coated with Y2SrAl4SiO12 conversion films	6.712	2419	12.240	75.377					
EVA film	39.67±0.17	2305	13.19	72.11	-1.2	1.0	3.5	10.1016/j.energy.2023.127354	2023
0.050 wt%CQDs/EVA	39.19±0.13	2390	13.65	72.86					
Glass	18.67	1103	15.53	75.4	2.57	0.26	3.15	10.1039/C8TA12519H	2019
2-layers N-GQD	19.15	1106	16.02	75.6					
Naked sc-Si solar cell	38.15±0.18	587±7	14.71	65.6	3.5	3.5	5.7	This work	
sc-Si cells covered with CAS/APCDs film	39.47±0.17	566± 6	15.55	67.9					

References

1. L. Mascaretti, Y. Chen, O. Henrotte, O. Yesilyurt, V. M. Shalaev, A. Naldoni and A. Boltasseva, *ACS Photonics*, 2023, **10**, 4079-4103.
2. H. K. Raut, V. A. Ganesh, A. S. Nair and S. Ramakrishna, *Energ Environ Sci*, 2011, **4**, 3779.
3. D. P. Sheehan, *J Non-Equil Thermody*, 2018, **43**, 301-315.
4. A. Zhou, Z. Yu, C. L. Chow and D. Lau, *Energy Build.*, 2017, **138**, 641-647.